

Supplement of Atmos. Chem. Phys., 14, 10267–10282, 2014
<http://www.atmos-chem-phys.net/14/10267/2014/>
doi:10.5194/acp-14-10267-2014-supplement
© Author(s) 2014. CC Attribution 3.0 License.



Supplement of

Size-resolved cloud condensation nuclei (CCN) activity and closure analysis at the HKUST Supersite in Hong Kong

J. W. Meng et al.

Correspondence to: C. K. Chan (keckchan@ust.hk)

27 **1 Uncertainty of N_{CN} , N_{CCN} , κ_{CCN} and κ_{AMS}**

28 The relative uncertainty of N_{CN} (ε_{CN}) is mainly determined by the uncertainty in the flow
29 rate (10%) and number counting (10%) of TSI 3785 WCPC, and the overall ε_{CN} is 14%. The
30 relative N_{CCN} (ε_{CCN}) uncertainty depends on the concentration-dependent Poisson statistical
31 uncertainty and the CCNc flow rate uncertainty (Moore et al., 2012; Roberts and Nenes, 2005):

$$32 \quad \varepsilon_{\text{CCN}}^2 = \varepsilon_{Q_{\text{CCN}}}^2 + \frac{\tau_{\text{CCN}}}{N_{\text{CCN}}Q_{\text{CCN}}} \quad (1)$$

33 where τ_{CCN} is the integration time (1 second) of CCNc optical particle counter (OPC) and Q_{CCN}
34 is the sample flow rate of CCNc ($45 \text{ cm}^3 \text{ min}^{-1}$), the $\varepsilon_{Q_{\text{CCN}}}$ is about 5%. Overall, ε_{CCN} increases
35 with the decrease of SS , since the N_{CCN} decreases as SS decreases. The maximum uncertainty is
36 $\sim 38\%$ at $SS = 0.15\%$ in this study.

37 The uncertainty of κ_{CCN} comes from the accuracy of the dry particles classified by the DMA
38 and the uncertainty of the activation efficiency ($\varepsilon_{\text{CCN}/\text{CN}}$) used for D_{50} determination. The
39 $\varepsilon_{\text{CCN}/\text{CN}}$ can be obtained from

$$40 \quad \varepsilon_{\text{CCN}/\text{CN}}^2 = \varepsilon_{\text{CN}}^2 + \varepsilon_{\text{CCN}}^2 \quad (2)$$

41 The sizing accuracy of DMA was determined by the accuracy of DMA sheath flow rate and
42 classifying voltage. The typical value is less than 3% (Wang et al. 2003). The overall uncertainty
43 in derived κ_{CCN} ranges from 23% to 39%.

44 The uncertainty of κ_{AMS} comes from the uncertainty in κ_{CCN} (as κ_{org} and κ_{inorg} are derived from
45 κ_{CCN} shown in main text), as well as the species densities and the volume fractions of organics
46 and inorganics that are derived from the AMS mass concentrations. The uncertainty of
47 inorganic compositions densities could be considered negligible. For organics, a mean value of
48 1.36 ± 0.11 for H:C and 0.40 ± 0.11 for O:C were found (Lee et al., 2013), and the organic
49 density estimated from the ratio of O:C ranging from 0.29 to 0.46 and H:C ranging from 1.49 to
50 1.28 were from 1.15 g cm^{-3} to 1.35 g cm^{-3} (Kuwata et al., 2011). The uncertainty of an assumed
51 organic density of 1.3 g cm^{-3} is less than 8%, which is smaller than the uncertainty in mass
52 concentrations ($\sim 30\%$) measured by AMS because of the uncertainty in collection efficiency

53 (*CE*) (Middlebrook et al., 2012). The large fractions of semi-volatile oxygenated organics
54 aerosols (SV-OOA) (23.5%) and low-volatile oxygenated organic aerosols (LV-OOA) (53.9%)
55 suggested that particles were largely aged and likely internally mixed. An internal mixing state
56 implies that the influences of *CE* on both NR inorganic and organic species are in the same
57 degree, thus have little impact on the derived volume fractions. In all, an uncertainty of 16% is
58 estimated for determination of inorganics and organics volume fractions, which are mainly due
59 to the uncertainties in relative ionization efficiency (*RIE*) (Bahreini et al., 2009; Mei et al.,
60 2013). The signal-to-noise ratio of the AMS data concerned, i.e. the ratio of mass
61 concentrations for the measurement period to that for the filter period, was higher than 6 for this
62 particle size range. It is worth noting that the low signal-to-noise ratios of AMS measurements
63 for small particles ($D_m < 50$ nm) will cause high uncertainty in κ_{AMS} derivation.

64

65

66 2 Supporting Figures

67

68

69

70

71

72

73

74

75

76

77

78

79

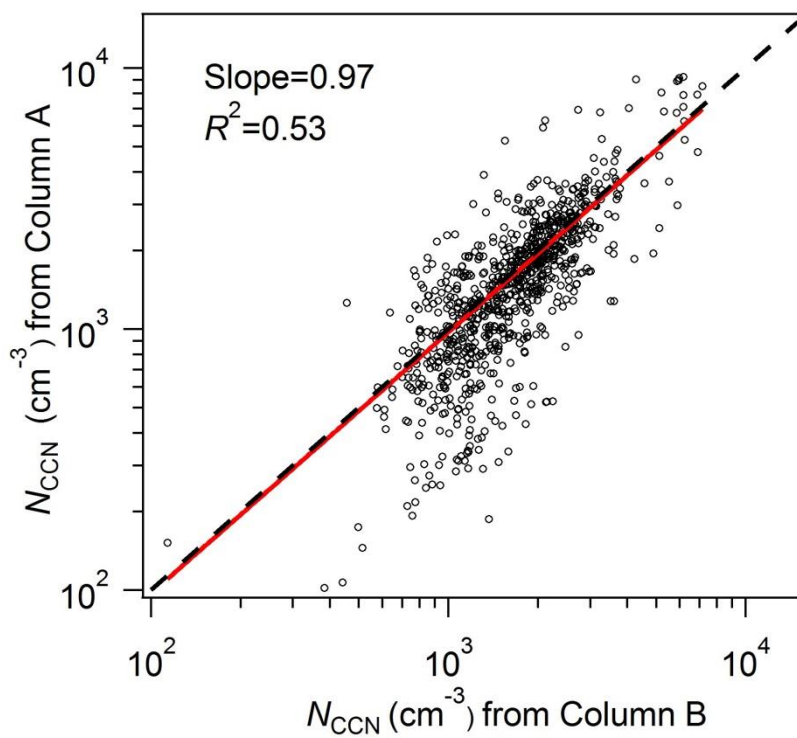
80

81

82

83

84



85 Fig.S1 Correlation of N_{CCN} from size-resolved CCN measurement (Column A) and bulk
86 measurement (Column B).

87

88

89

90

91

92

93

94

95

96

97

98

99

100

101

102

103

104

105

106

107

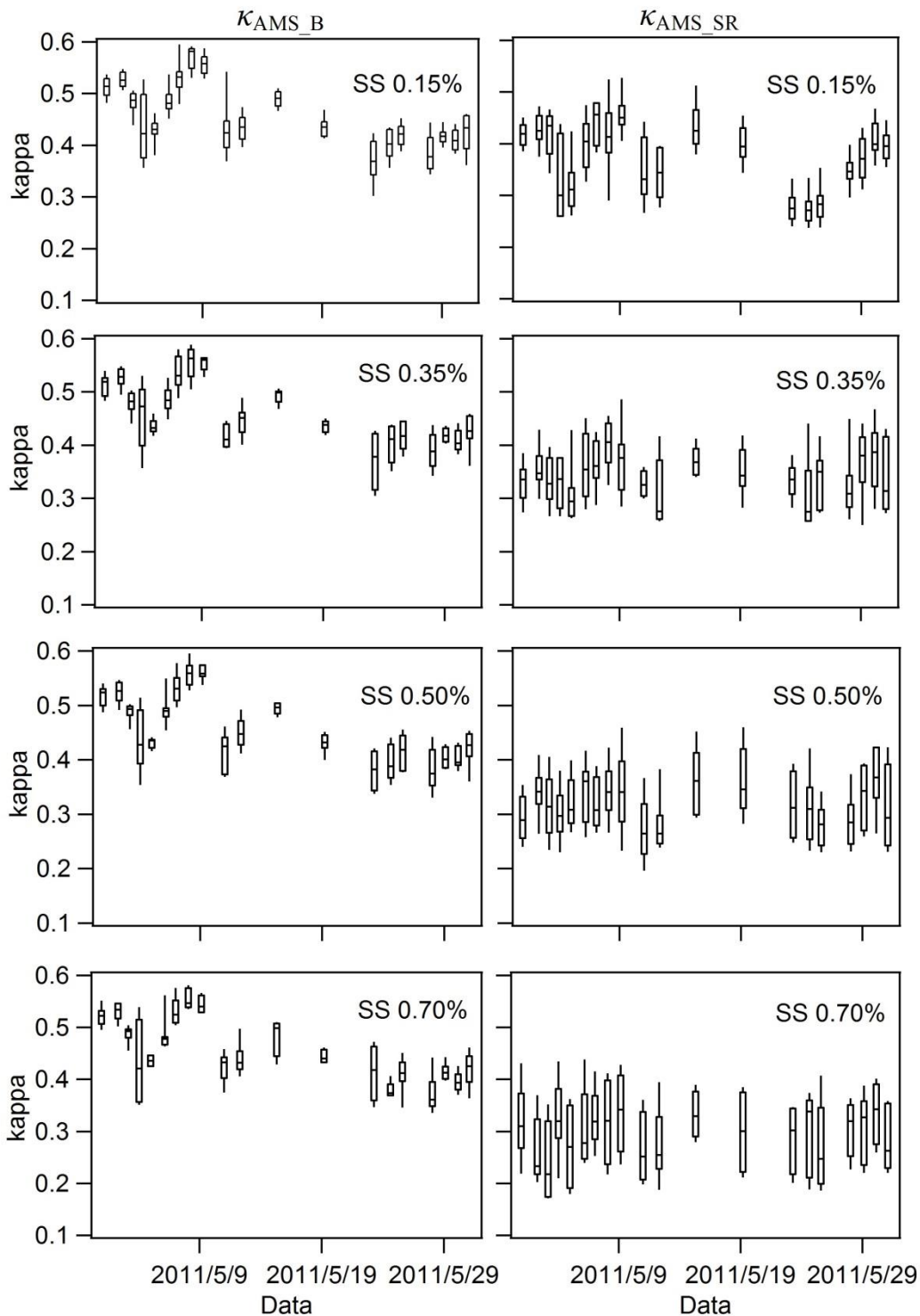


Fig.S2 The bulk κ_{AMS} (κ_{AMS_B}) and the size-resolved κ_{AMS} (κ_{AMS_SR}) derived from AMS measurement.

108

109

110

111

112

113

114

115

116

117

118

119

120

121

122

123

124

125

126

127

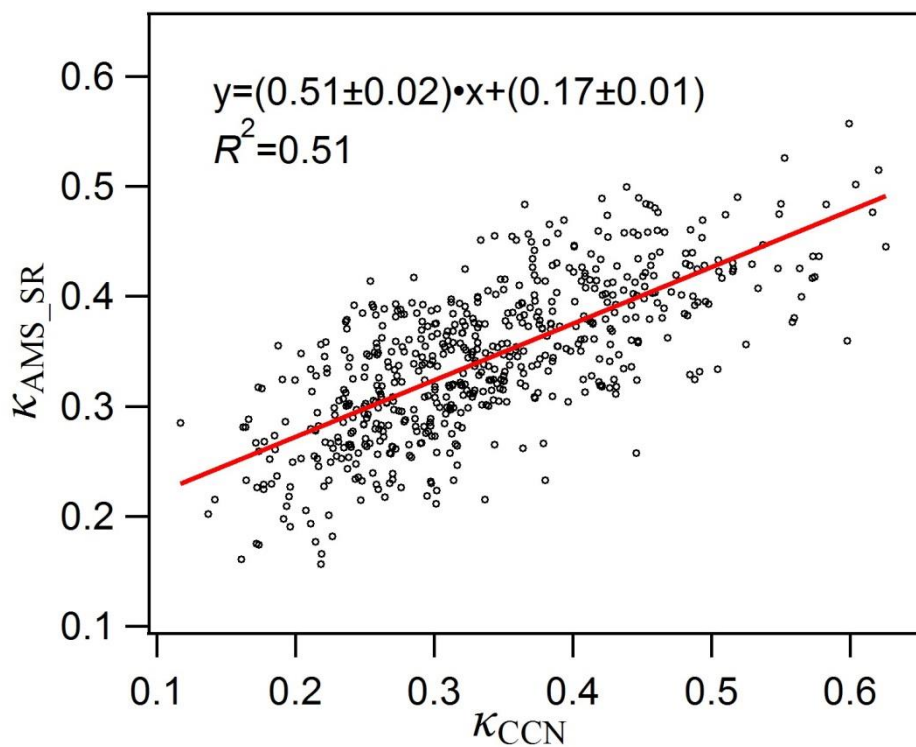
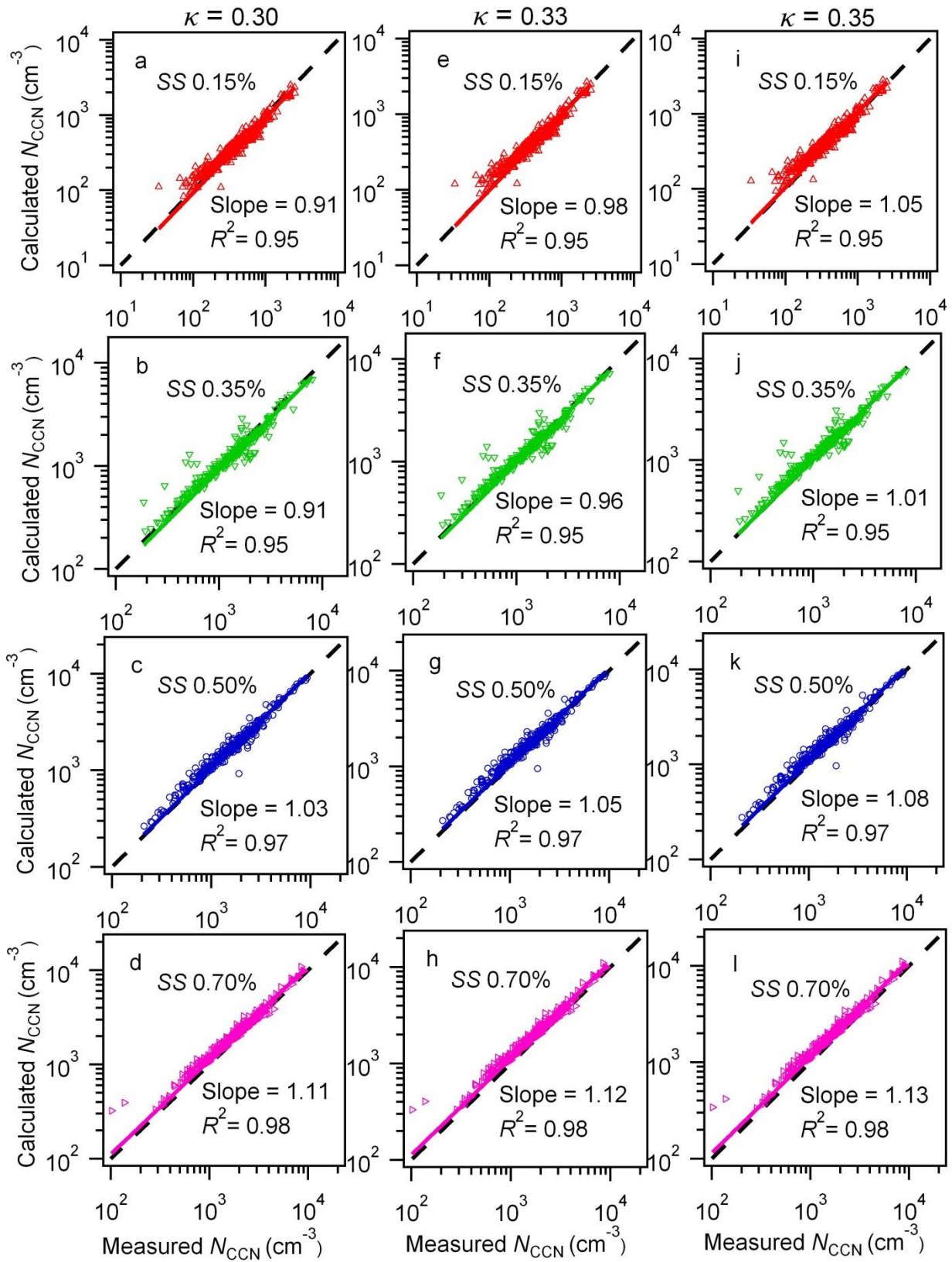


Fig.S3 Correlation of κ_{CCN} derived from CCN measurement and κ_{AMS_SR} from AMS measurement.



128 Fig.S4. Predictions of N_{CCN} based on D_{50} derived from constant κ of (a-d) 0.30, (e-h) 0.33 and (i-
 129 l) 0.35 during whole period, respectively.

130
 131
 132
 133
 134
 135
 136
 137
 138
 139
 140
 141
 142
 143
 144
 145
 146
 147
 148
 149
 150

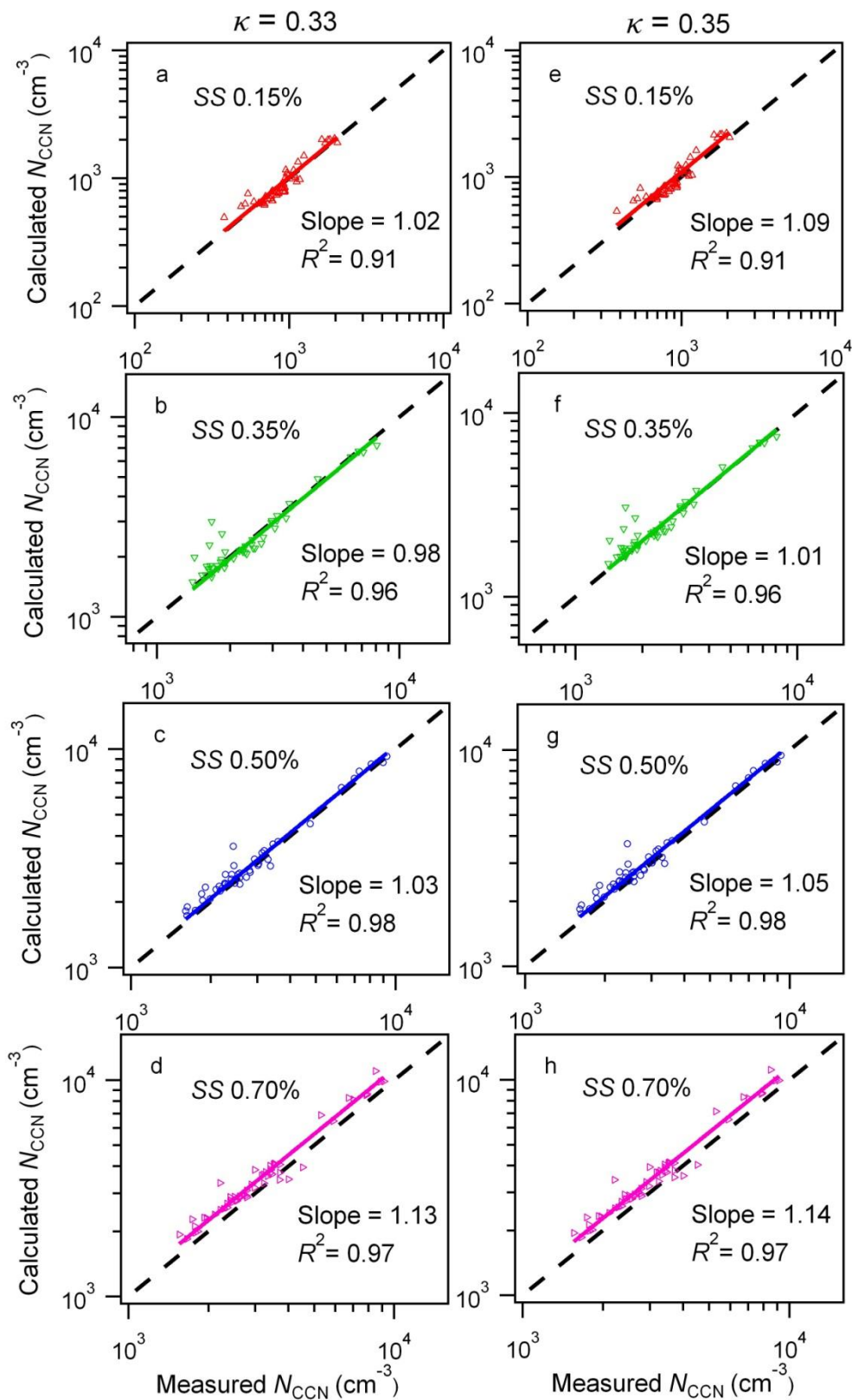
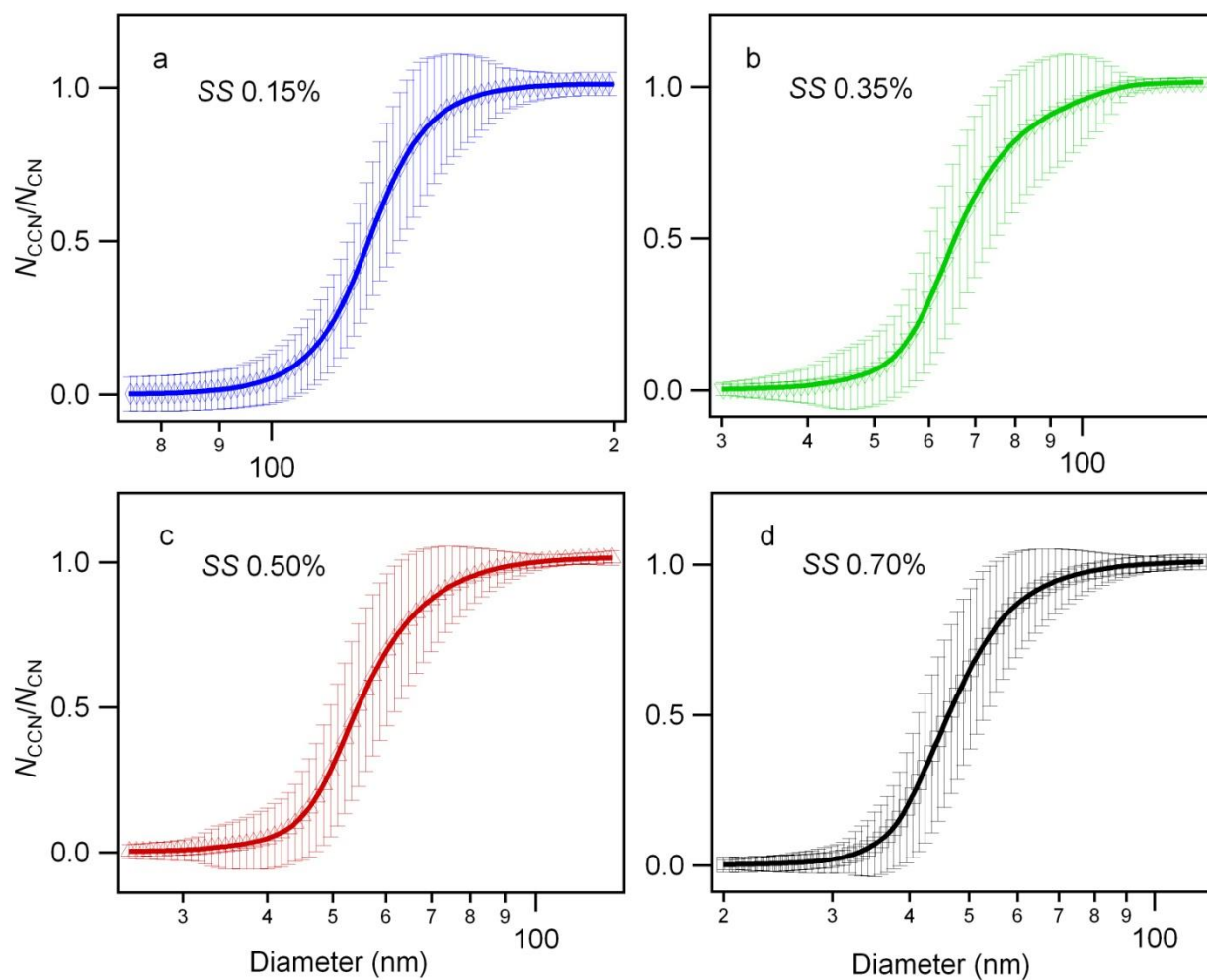


Fig.S5. Predictions of N_{CCN} based on D_{50} derived from constant κ of (a-d) 0.33 and (e-h) 0.35 during hazy period.



151
 152
 153
 154
 155
 156
 157
 158
 159
 160

Fig.S6. The average size-resolved CCN activation ratio at SS (a) 0.15%, (b) 0.35%, (c) 0.50% and (d) 0.70%.

161 **References**

- 162 Bahreini, R., Ervens, B., Middlebrook, A., Warneke, C., de Gouw, J., DeCarlo, P., Jimenez, J.,
163 Brock, C., Neuman, J., and Ryerson, T.: Organic aerosol formation in urban and industrial
164 plumes near Houston and Dallas, Texas, *J. Geophys. Res.*, 114, D00F16,
165 doi:10.1029/2008JD011493, 2009.
- 166 Kuwata, M., Zorn, S. R., and Martin, S. T.: Using elemental ratios to predict the density of
167 organic material composed of carbon, hydrogen, and oxygen, *Environ. Sci. Technol.*, 46, 787-
168 794, 2011.
- 169 Lee, B. P., Li, Y. J., Yu, J. Z., Louie, P. K., and Chan, C. K.: Physical and chemical
170 characterization of ambient aerosol by HR-ToF-AMS at a suburban site in Hong Kong during
171 springtime 2011, *J. Geophys. Res.-Atmos.*, 118, 8625-8639, doi:10.1002/jgrd.50658, 2013.
- 172 Mei, F., Setyan, A., Zhang, Q., and Wang, J.: CCN activity of organic aerosols observed
173 downwind of urban emissions during CARES, *Atmos. Chem. Phys.*, 13, 12155-12169,
174 doi:10.5194/acp-13-12155-2013, 2013.
- 175 Middlebrook, A. M., Bahreini, R., Jimenez, J. L., and Canagaratna, M. R.: Evaluation of
176 composition-dependent collection efficiencies for the Aerodyne aerosol mass spectrometer
177 using field data, *Aerosol Sci. Technol.*, 46, 258-271, 2012.
- 178 Moore, R. H., Raatikainen, T., Langridge, J. M., Bahreini, R., Brock, C. A., Holloway, J. S.,
179 Lack, D. A., Middlebrook, A. M., Perring, A. E., and Schwarz, J. P.: CCN spectra,
180 hygroscopicity, and droplet activation kinetics of secondary organic aerosol resulting from the
181 2010 Deepwater Horizon oil spill, *Environ. Sci. Technol.*, 46, 3093-3100, 2012.
- 182 Roberts, G. and Nenes, A.: A continuous-flow streamwise thermal-gradient CCN chamber for
183 atmospheric measurements, *Aerosol Sci. Technol.*, 39, 206-221, 2005.
- 184 Wang, J., Flagan, R. C., and Seinfeld, J. H.: A differential mobility analyzer (DMA) system for
185 submicron aerosol measurements at ambient relative humidity, *Aerosol Sci. Technol.*, 37, 46-
186 52, 2003.

187

188

189

190

191